Ecotoxicology and Environmental Safety 309 (2026) 119570

Contents lists available at ScienceDirect

Ecotoxicology and Environmental Safety

journal homepage: www.elsevier.com/locate/ecoenv

Quantifying the multi-year impacts of Indo-China Peninsula biomass burning on vegetation gross primary productivity in southern China

Wenjie Yan, Jun Zhu *, Xu Yue, Chenguang Tian, Yonghang Hu, Jiao Zheng, Yihan Hu, Yuan Zhao, Xin Chen, Sheng Yang, Haoyu Wei, Hong Liao

Jiangsu Key Laboratory of Atmospheric Environment Monitoring and Pollution Control, Jiangsu Collaborative Innovation Center of Atmospheric Environment and Equipment Technology, School of Environmental Science and Engineering, Nanjing University of Information Science & Technology (NUIST), Nanjing 210044, China

ARTICLE INFO

Edited by Guorui Liu

Keywords:
Fire aerosols and ozone
Pollution transport
Gross primary productivity

ABSTRACT

Biomass burning (BB) emissions in the Indo-China Peninsula (ICP) can be transported to southern China, perturbing the atmospheric environment and climate in southern China. However, the impact of these fire emissions transports on the terrestrial ecosystems in southern China remains unclear. Here we combine several state-of-the-art models and multiple measurement datasets to quantify the impacts of ICP fire-induced aerosol radiation and O_3 damage effect on gross primary productivity (GPP) in southern China during ICP fire seasons (March and April) in 2013–2019. Our results demonstrate that ICP fire-derived aerosols and O_3 collectively reduce annual mean GPP in southern China by 5.4 % (-13.86 TgC per burning season) under all-sky and 3.4 % (-12.87 TgC per burning season) under clear-sky conditions. In all-sky, fire aerosols decreased direct photosynthetically active radiation (PAR) by 2.68 W m^{-2} while increased diffuse PAR marginally (+0.03 W m^{-2}), driving a GPP reduction of 13.36 TgC per burning season across southern China. Concurrently, fire-induced O_3 reduces regional GPP by 0.54 TgC per burning season. In clear-sky, aerosols reduce direct PAR more sharply (−3.22 W m^{-2}) but enhance diffuse PAR (+1.51 W m^{-2}), resulting the GPP loss to 12.18 TgC, while O_3 damage effect is increased (−0.69 TgC). The fire aerosols contributed to 96.4 % of the GPP reduction in all-sky and 94.6 % in clear-sky, whereas ozone played a minor role (3.9 % in all-sky and 5.4 % in clear-sky). This study highlights ICP fire emissions as a significant driver of ecosystem productivity declines in downwind regions, influencing the regional land carbon cycle.

1. Introduction

Fire emissions represent a significant global source of trace gases and aerosols, which have demonstrable impacts on regional air quality, climate, and terrestrial ecosystems through complex atmospheric transport processes (Park et al., 2024; Wei et al., 2023; Yin et al., 2020). Recent research in observational technologies, combined with advancements in atmospheric modeling frameworks and the integration of machine learning techniques, has enabled more accurate quantification of the impacts of fire emissions (Coen, 2018; Hung et al., 2021; Lu et al., 2019). These developments have highlighted significant knowledge gaps concerning the ecosystem-scale consequences of fire pollution transport, particularly its impact on gross primary productivity (GPP) in downwind areas.

Researches have documented significant impacts of fire smoke transport on a global scale (Brown et al., 2021; Wotawa and Trainer, 2000) and in various regions with frequent fire activities, such as South America (Pereira et al., 2009), the Amazon (Bencherif et al., 2020; Videla et al., 2013), the Indian Peninsula (Bhawar et al., 2024), and the Siberian forests (Kommula et al., 2024; Tian et al., 2023; Youn et al., 2011). Spring biomass burning (BB) in Southeast Asia is frequent, particularly in the Indo-Chinese Peninsula (ICP) during March and April, resulting in significant aerosol and ozone (O_3) from fire emissions (Chang et al., 2015; Tsay et al., 2013). These ICP fires, caused by agricultural and natural factors, significantly degrade regional air quality and impact atmospheric brown clouds and precipitation (Lin et al., 2014b; Reddington et al., 2021, 2014; Wang et al., 2022; Zheng et al., 2023).

Previous results indicated that fire emissions in the Indo-Chinese Peninsula (ICP) significantly affect the air quality in southern China (Chan et al., 2003; Huang et al., 2013; Lin et al., 2014a; Zhang et al., 2022; Zhu et al., 2024). Researches shown that fire emissions from ICP

* Corresponding author.
E-mail address: junzhu@nuist.edu.cn (J. Zhu).

https://doi.org/10.1016/j.ecoenv.2025.119570
Received 9 September 2025; Received in revised form 28 November 2025; Accepted 11 December 2025
Available online 15 December 2025

region contribute approximately 10–70 % of $PM_{2.5}$ in southern China (Fan et al., 2023; Li et al., 2017a; Yang et al., 2022; Zhang et al., 2021; Zhu et al., 2022), and increase O_3 concentrations by as much as 10–30 % (Choi and Ying, 2025; Fu et al., 2012). Besides its influence on the atmospheric environment, the smoke aerosol transported to southern China significantly impacts the region's weather and climate (Chen et al., 2017; Ding et al., 2013; Huang et al., 2016). The ICP fire aerosols transported to southern China heat the atmosphere while cooling the surface by reducing shortwave radiation at the ground to between 4 and 20 W/m^2 (Kong et al., 2022; Lin et al., 2014a; Zhu et al., 2024). Additionally, they can modulate cloud formation and precipitation in southern China (Cohen et al., 2017; Li et al., 2024).

Previous extensive research demonstrates that the Indo-Chinese Peninsula (ICP) fire-induced aerosols and ozone have significant impacts on local and downwind atmospheric environments and climate (Azevedo et al., 2011; Hein et al., 2022). However, the transregional effects of these pollutants on ecosystem health and carbon cycling remain poorly quantified. These pollutants impact vegetation through distinct mechanisms: aerosols modify photosynthesis by altering radiation and causing meteorological disturbances (Chen and Zhuang, 2014b; Mahowald, 2011; Yue et al., 2017), while ozone penetrates stomata, damaging the photosynthetic apparatus and reducing productivity in both crops and forests (Feng et al., 2018, 2022). Although the opposing effects of transported fire pollution on Amazonian vegetation have been documented (Martins et al., 2018), the overall impact on ecosystems in fire-emission hotspots, such as the ICP region, remains unknown.

This raises interesting questions: How much do the Indo-Chinese Peninsula (ICP) biomass burning induced aerosols and ozone contribute to vegetation productivity in southern China during the ICP peak fire season (March and April)? To address the question above, we quantify the net impacts of ICP fire aerosols and O_3 on ecosystem vegetation gross primary productivity (GPP) in southern China by utilizing a combination of multi-source observations and a suite of validated models. The chemical transport model GEOS-Chem (Wang et al., 1998) is used to predict fire-induced changes in aerosol optical depth and surface ozone. The Column Radiation Model (CRM) is applied to quantify perturbations in diffuse and direct solar radiation caused by fire aerosols. The Interactive Model of Air Pollution and Land Ecosystems (IMAPLE)(Yue et al., 2024), a dynamic global vegetation model, is used to quantify changes in ecosystem GPP resulting from the effects of aerosol radiation and O_3 inhibition caused by transported fire aerosols and ozone pollution. Section 2 outlines the research region, methods, and data. Section 3 examines the variations in photosynthetically active radiation (PAR) due to biomass burning, the effects of biomass burning on GPP, and the respective contributions of fires aerosol and O_3 from ICP to GPP in southern China.

2. Research region, methods and data

2.1. Research region

Our analysis focuses on three southern Chinese provinces adjacent to the Indo-Chinese Peninsula (ICP): Yunnan (YN), Guangxi (GX), and Guangdong (GD), which form a continuous geographical corridor from west to east (Fig. 1a). This region is a key area affected by the transboundary transport of pollutants from Southeast Asia (Yin et al., 2021), making it highly suitable for investigating the transport of regional pollutants and their ecological impact processes. The total carbon storage of the forest vegetation in this region accounts for approximately 20 % of the total carbon storage in all of the entire China, underscoring its critical role in the national carbon balance (Lan et al., 2019; Haofan et al., 2019; Zhang et al., 2010; Zhang Yuxing and Pu., 2021). To evaluate the effects of aerosols and ozone on vegetation, we utilized observational data from 51 monitoring stations operated by China's Ministry of Ecology and Environment (CMEE) throughout the study area. These stations provide high-resolution measurements of key atmospheric composition variables such as $PM_{2.5}$ and O_3, and enhance this analysis by offering ground data to validate model outputs. These regions were selected because of their downwind position relative to prevailing springtime transport patterns. The ICP region includes Myanmar, Thailand, Laos, Vietnam, and Cambodia. There are frequent fire activities during the late dry season and the transition from the dry to the wet season in the ICP region, due to slash-and-burn and land-clearing practices. Peak activity consistently occurs during the fire season in March and April. Thus, this study specifically focuses on the late dry season (March–April), which coincides with the biomass burning period in the ICP. Fig. 1b illustrates the interannual variability of biomass burning in the ICP, displaying monthly averages from 2010 to 2020.

2.2. Chemical transport model GEOS-Chem

Goddard Earth Observing System coupled with Chemistry (GEOS-Chem, https://geoschem.github.io/) is a global three-dimensional atmospheric chemistry and transport model that simulates the distribution of gaseous pollutants and aerosols. It incorporates comprehensive chemical mechanisms, including reactions involving $HO_x - NO_x - VOC - O_3$. The model simulates key aerosol components, including black carbon (BC), organic carbon (OC), sulfate, nitrate, dust, and sea salt in both coarse and accumulation modes. In this study, we used version 12.0.0 of the GEOS-Chem model (with a horizontal resolution of

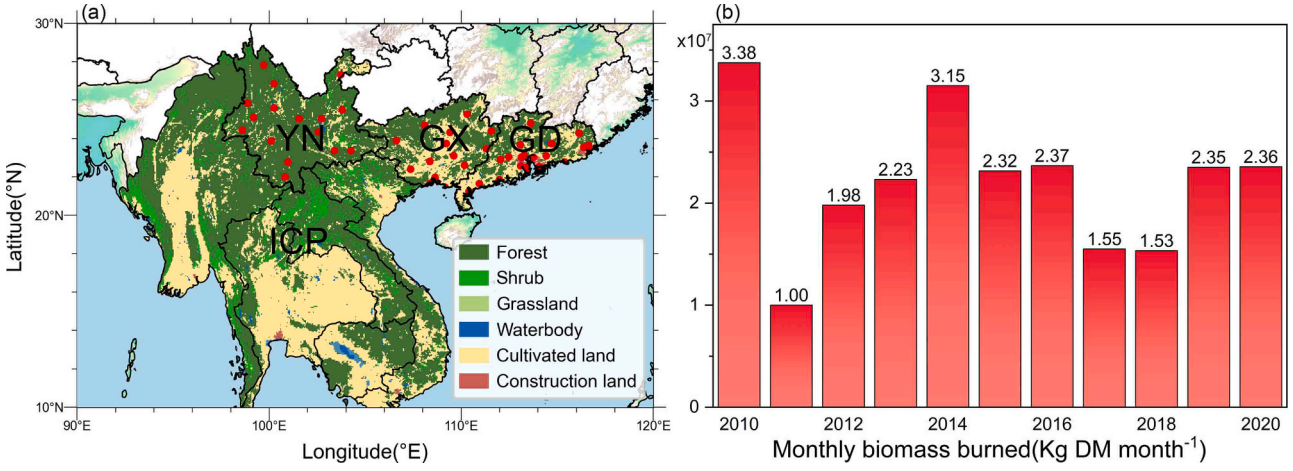

Fig. 1. (a) Topography of the study regions and the 51 $PM_{2.5}$ and ozone ground-based stations from CMEE (red dots) for model evaluation; (b) Monthly biomass burning during the burning season (March–April) of 2013–2019 in the Indo-Chinese Peninsula (ICP).

2° × 2.5° and 47 vertical layers), with 2012 as the spin-up period, to simulate the three-dimensional distribution of aerosols and ozone concentrations from 2013 to 2019. The model was driven by MERRA-2 reanalysis data provided by the Global Modeling and Assimilation Office (GMAO), with meteorological fields updated every three hours and surface parameters updated hourly. Emission data processing was conducted using the Harvard-NASA Emissions Component (HEMCO), developed by Keller et al. (2014). Anthropogenic emissions in East Asia were sourced from the MIX inventory published by Li et al. (2017)b, while biomass burning emissions were obtained from the Global Fire Emissions Database, version 4 s (GFED4s), GFED4s was integrated into the GEOS-Chem model using the HEMCO module (Lin et al., 2021). For the transport processes, the model employed the TPCORE advection scheme developed by Lin and Rood (1996). Convective transport was calculated using the method proposed by Wu et al. (2007), which employs convective mass fluxes derived from meteorological fields. The mixing within the planetary boundary layer was addressed using the non-local mixing scheme developed by Lin and McElroy (Lin and McElroy, 2010). Dry deposition of gases followed the scheme proposed by Wesely (1989), as implemented by Wang et al. (1998), while aerosol deposition was based on the parameterization developed by Zhang et al. (2001). Wet deposition was addressed using the methodology outlined by Liu et al. (2001). By relying on the default GEOS-Chem parameterization scheme, we did not consider the impacts of plume rise in the model. Previous studies have shown that the GEOS-Chem model can effectively replicate the spatial and temporal distribution patterns of $PM_{2.5}$ and O_3 across China (Hu et al., 2023; Jiang et al., 2020).

2.3. Radiative transfer model

The Column Radiation Model (CRM) is an independent radiative transfer module developed from the NCAR Community Climate System Model (http://www.cesm.ucar.edu/models/). The model explicitly simulates the direct radiative effects of aerosols, encompassing both absorption and scattering processes. These calculations are conducted hourly across 20 vertical layers, extending from the surface up to 0.5 hPa (Yue and Unger, 2017). The CRM integrates various aerosol vertical distribution data provided by the GEOS-Chem model, including sulfate, nitrate, black carbon (BC), organic carbon (OC), mineral dust (which includes clay and silt), and sea salt (categorized into coarse and accumulation modes). The aerosol optical properties of sea salt(e.g., single scattering albedo, extinction coefficient, and asymmetry factor) were obtained from the work of Yue and Liao (2012). The optical parameters for mineral dust were derived from on Yue et al. (2010), while the parameters for other aerosol species were obtained from the RegCM4 model (Giorgi et al., 2012). In this study, the CRM was used to evaluate the impact of aerosols on surface radiative fluxes, specifically their influence on both diffuse and direct photosynthetically active radiation (PAR). The meteorological input data for the model were sourced from the MERRA-2 reanalysis product, which has a spatial resolution of 1° × 1° and a temporal resolution of one hour. Additionally, hourly cloud fraction and liquid water path data from the CERES SYN1deg dataset were included.

2.4. Interactive model for air pollution and land ecosystems

The Interactive Model for Air Pollution and Land Ecosystems (IMAPLE) (Yue et al., 2024) simulates surface energy exchange as well as carbon and water cycling within the biosphere. It is built upon the well-validated Yale Interactive Terrestrial Biosphere model (YIBs) (Yue et al., 2015). In its latest version, the model incorporates trait-based ozone damage and process-based modules for hydrological cycling, wetland methane emissions, and fire emissions. The model can dynamically simulate carbon fluxes, leaf area index, tree growth, and carbon allocation for nine plant functional types, as well as prognostic soil temperature, soil moisture, and evapotranspiration. IMAPLE model focuses on refining the following key ecological processes: two-leaf radiative transfer, the coupling of carbon and water fluxes (simulating the pathway of aerosol climate impacts), and stomatal uptake processes (simulating the pathway of ozone damage to vegetation). Since 2020, IMAPLE (and the earlier version of the YIBs model) has participated in the multi-model ensemble project TRENDY to provide estimates of the global carbon budget. The Global Carbon Budget 2024 (Friedlingstein et al., 2025) demonstrated that the IMAPLE model performs effectively well in assessing key carbon and water fluxes. For the IMAPLE model, we set the spin-up period as 2003–2012, and the formal analysis is based on the simulation data from 2013 to 2019.

2.5. Model simulations

We perform two GEOS-Chem runs, along with four the Column Radiation Model (CRM) and the Interactive Model of Air Pollution and Land Ecosystems (IMAPLE) runs (Table 1), to isolate the effects of fire aerosols on both direct and diffuse radiation under varying sky conditions, and to assess their subsequent impacts on gross primary productivity (GPP) (Fig. 2). Both the BASE and TEST experiments utilized the MIX inventory (Li et al., 2017b) for anthropogenic emissions over East Asia, with the Global Fire Emissions Database, version 4 s (GFED4s) supplying biomass burning emissions. The key distinction between the experiments was the exclusion of fire emissions from the Indochina Peninsula (ICP) in the TEST experiment. The CRM simulations aimed to quantify variations in photosynthetically active radiation (PAR) induced by aerosols, using aerosol profiles simulated by GEOS-Chem. These calculations were performed under two distinct sky conditions: CLD runs (all-sky conditions) incorporated observed cloud profiles, while CLR runs (clear-sky conditions) assumed no cloud cover. Finally, PAR values served as inputs to the IMAPLE model for to simulate GPP variations induced by the aerosol radiation effect. The IMAPLE simulations also incorporated ozone concentration data from GEOS-Chem outputs to assess reductions in GPP caused by ozone. During IMAPLE model simulations, meteorological fields, CO_2 concentrations, and land cover were fixed at initial year (2013) levels to eliminate the synergistic influence of these variables on the experiments. To quantify the relative contributions of aerosols and ozone to the total GPP loss, we calculated the contribution rate of each factor. The specific formulas are as follows:

$$\Delta GPP = GPP_{Fire} - GPP_{NoFire}$$

$$Contribution\ of\ Aerosols(\%) = \frac{\Delta GPP_{aerosols}}{\Delta GPP_{aerosols} + \Delta GPP_{ozone}} \times 100\%$$

$$Contribution\ of\ Ozone(\%) = \frac{\Delta GPP_{ozone}}{\Delta GPP_{aerosols} + \Delta GPP_{ozone}} \times 100\%$$

GPP_{Fire}: GPP under the ICP region fire.

GPP_{NoFire}: GPP under the ICP region no fire.

$\Delta GPP_{aerosols}$: the change in GPP induced only by aerosol under the ICP region fire and no fire emission.

ΔGPP_{ozone}: the change in GPP induced only by ozone under the ICP region fire and no fire emission.

2.6. Observations data

In this study, the performance of the GEOS-Chem model was evaluated using daily mean $PM_{2.5}$ and O_3 concentrations provided by China's Ministry of Ecology and Environment (CMEE, https://www.cnemc.cn/) at 51 ground-based monitoring stations across Yunnan, Guangdong, and Guangxi provinces. Additionally, aerosol optical depth (AOD) data from the Moderate Resolution Imaging Spectroradiometer (MODIS, https://modis.gsfc.nasa.gov) were used to evaluated the AOD simulation from the Column Radiation Model (CRM) radiation transfer model, and shortwave and diffuse radiation data from the CERES SYN1deg product (http://ceres.larc.nasa.gov) were downscaled to a 1° × 1° spatial

Table 1
Summary of simulations and research flow chart.

Simulations	Models	Period	Input	Cloud	O_3 effects	Output
BASE	GEOS-Chem	2012–2019	All emissions	Obs.	None	Monthly 3-D aerosol concentrations and O_3
TEST			All without ICP fire emissions			
CRM_BASE_CLD	CRM	2013–2019	Aerosols from BASE	Obs.	None	Hourly direct and diffuse PAR at surface
CRM_TEST_CLD			Aerosols from TEST			
CRM_BASE_CLR			Aerosols from BASE	None		
CRM_TEST_CLR			Aerosols from TEST			
IMAPLE_BASE_CLD	IMAPLE	2003–2019	PAR from CRM_BASE_CLD	Obs.	Input O_3 from GEOS-Chem simulations	Monthly GPP
IMAPLE_TEST_CLD			PAR from CRM_TEST_CLD			
IMAPLE_BASE_CLR			PAR from CRM_BASE_CLR	None		
IMAPLE_TEST_CLR			PAR from CRM_TEST_CLR			

*The GEOS-Chem model outputs daily data with a resolution of 2°× 2.5°, while the CRM and IMAPLE models output daily data with a resolution of 1°× 1°.

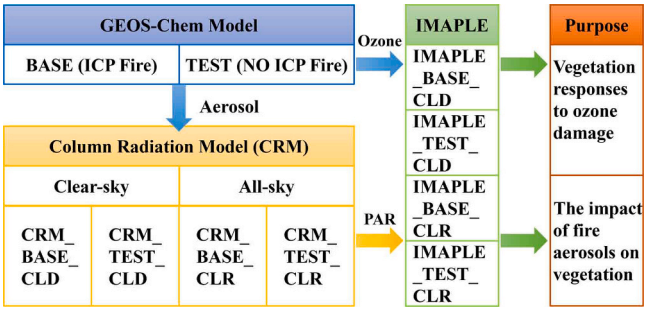

Fig. 2. Flow chart of modelling methods.

resolution on a monthly basis and used to validate the radiation fluxes simulated by the CRM radiation transfer model. Satellite-derived gross primary productivity (GPP) data at a 0.25° × 0.25° resolution from the GLASS product (https://www.glass.umd.edu/LAI/MODIS/0.25D/) for the period 2013–2019 were used to validate the dynamic vegetation model MAPLE. The GLASS GPP product, along with the biomass burned data from the Global Fire Emissions Database the Global Fire Emissions Database, version 4 s (GFED4s) (van der Werf et al., 2017), was also used to evaluate the contribution of fire emissions transport to GPP based on observations. The wind direction data used in this study were obtained from the ECMWF Reanalysis 5th Generation dataset (ERA5, https://www.ecmwf.int/), which provides hourly global atmospheric variables at high spatial resolution. To assess the model's performance, we used several statistical metrics, including the correlation coefficient (R), mean bias (MB), normalized mean bias (NMB), and root mean square error (RMSE), defined as follows:

$$R = \frac{\sum_{i=1}^{i=n}(M_i - \overline{M})(O_i - \overline{O})}{\sqrt{\sum_{i=1}^{i=n}(M_i - \overline{M})^2 \times \sum_{i=1}^{i=n}(O_i - \overline{O})^2}}, \quad (1)$$

$$MB = \frac{1}{n}\sum_{i=1}^{i=n}(M_i - O_i), \quad (2)$$

$$NMB = \frac{\sum_{i=1}^{i=n}(M_i - O_i)}{\sum_{i=1}^{i=n}O_i}\%, \quad (3)$$

$$RMSE = \sqrt{\sum_{i=1}^{i=n}\frac{(M_i - O_i)^2}{n}}, \quad (4)$$

Where O_i and M_i are observed and modeled values, respectively. $\overline{O}$ and $\overline{M}$ are the averages of the observed and modeled values. In this study, R, MB, NMB and RMSE are used to evaluate the performance of models on the spatial scale, and the student t test is used to examine the significance of correlation coefficients and long-term trends.

3. Results

3.1. Model evaluations

The evaluation of the simulation results from each model is presented in Fig. 3. Compared to the observed data, the GEOS-Chem model effectively reproduced the monthly $PM_{2.5}$ (Fig. 3a) and O_3 values (Fig. 3b) from the CMEE ground observations, with R of 0.51 ($p < 0.01$) for both variables. Similarly, the AOD from the the Column Radiation Model (CRM) model reproduces the observed spatial pattern from the MODIS product (Fig. 3c) with a high R of 0.64 ($p < 0.01$) and a low the mean bias (MB) of −0.19. The CRM, driven by aerosol concentrations from GEOS-Chem, exhibits shortwave radiation patterns similar to those observed by satellites (Fig. 3d–e). The simulations agree with observations well, with a high R of 0.82 and low NMB of −29.0 % under all-sky conditions, and with R of 0.92 and NMB of −10.6 % under clear-sky conditions. Although CRM presents high R and low NMB under both sky conditions, evaluations still show that model shortwave radiation is higher than observations. Such overestimation may be related to the underestimation of simulated AOD (Fig. 3c), which leads to more shortwave radiation reaching the surface. Additionally, the Interactive Model of Air Pollution and Land Ecosystems (IMAPLE) model simulates a reasonable spatial pattern of gross primary productivity (GPP) to the compared to GLASS product (Fig. 3f), with a high correlation coefficient (R) of 0.88 ($p < 0.01$) and a low NMB of 7.4 %. Overall, the suite of models we used—including GEOS-Chem, CRM, and IMAPLE—reasonably captures the temporal and spatial distribution of atmospheric pollutants (aerosols and ozone), aerosol radiation properties, and GPP over the study regions during March–April from 2013 to 2019.

3.2. Changes of GPP by fire emissions

The spatial distribution and annual variation of fire emission contributions to gross primary productivity (GPP) in the Indo-Chinese Peninsula (ICP) region across the three southern provinces of China from 2013 to 2019, under both all-sky and clear-sky conditions, are shown in Fig. 4. The results reveal that fire emissions transported from the ICP region during March and April suppress GPP across southern China, causing daily reductions of 0.28 gC m^{-2} d^{-1} (5.4 % annualized) under all-sky conditions and 0.26 gC m^{-2} d^{-1} (3.4 % annualized) under clear skies (Fig. 4a and b). These reductions cumulatively amount to 13.86 and 12.87 TgC per burning season, respectively. For the three regions in southern China, the contribution of ICP fire transport shows a consistent west-to-east attenuation of its effects, with maximum suppression in southern Yunnan that decreases with downwind distance under clear sky conditions. However, this phenomenon does not occur under all-sky conditions, which is attributed to the influence of clouds. Regarding the interannual variability of the contributions of ICP fire transport to GPP in southern China (Fig. 4c–d), the results indicate a decline in GPP from 2013 to 2019, with the greatest impact observed in

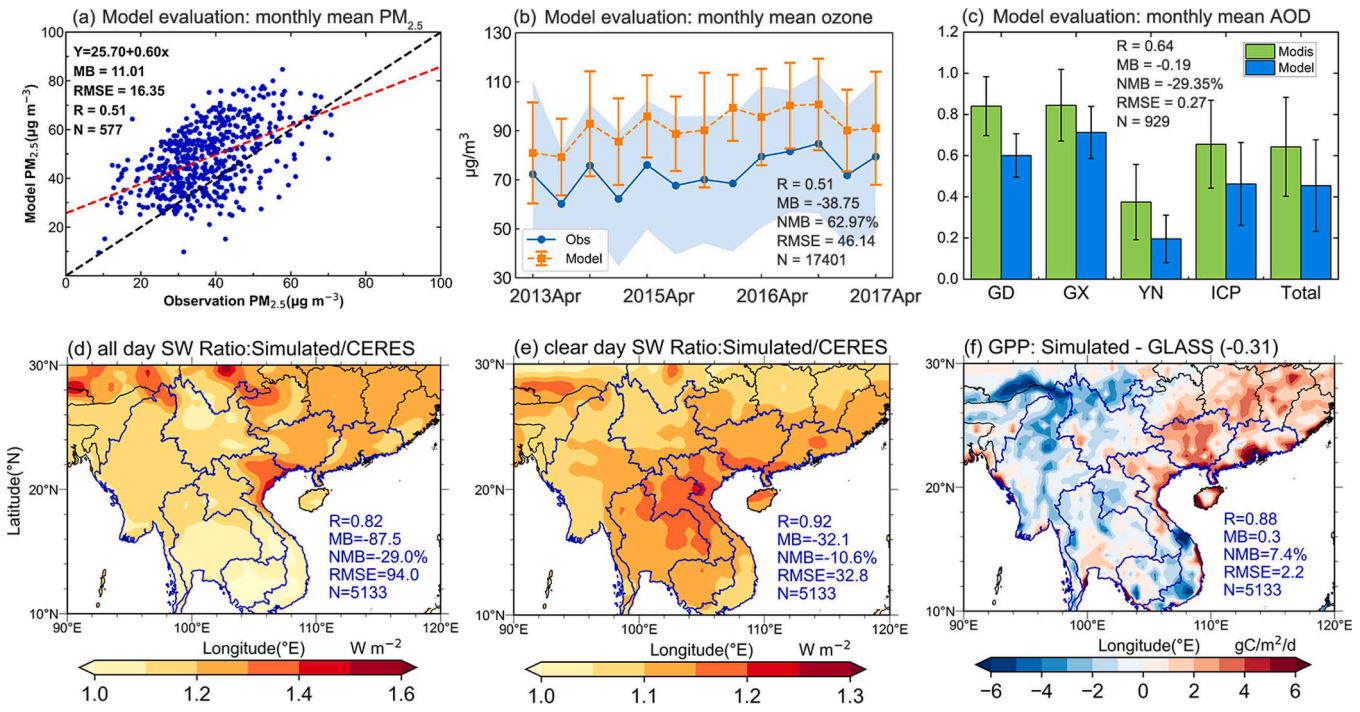

Fig. 3. Models' evaluation using ground-based and satellite observation during March-April from 2013 to 2019. GEOS-Chem monthly $PM_{2.5}$ (a) and ozone (b) evaluation by ground observation from CMEE at the 51 sites; (c) CRM regional monthly AOD evaluation using MODIS AOD; Evaluations of simulated monthly shortwave radiation (SW) by CRM model for (d) all-sky and (e) clear-sky; (f) Evaluation of simulated gross primary productivity (GPP) by IMAPLE model. The statistical parameters include the number of matchup data (N), the slope and intercept at the y axis of the linear regression (red line), the mean bias (MB), the root-mean-squared error (RMSE), the normalized mean bias (NMB), and the correlation coefficient (R).

2014 under both all-sky and clear-sky conditions, and the smallest reduction occurring in 2018. These interannual patterns show strong consistency with the temporal variations in biomass burned during the burning season (March–April) from 2013 to 2019 in ICP (Fig. 1b), suggesting that fire emissions in ICP were an important factor contributing to fire transport's impact on GPP in southern China.

This suppression of vegetation gross primary productivity (GPP) results from the combined effects of aerosol radiation and ozone damage, which will be comprehensively analyzed in the following section. While GPP typically correlates positively with the aerosol radiation effect, fire aerosols modify this relationship by simultaneously increasing diffuse radiation and decreasing direct radiation. The reduction of direct light can offset the benefits of diffuse fertilization, resulting in positive GPP responses at low to medium diffuse fractions but negative responses at high diffuse fractions. The Interactive Model of Air Pollution and Land Ecosystems (IMAPLE) model effectively captures the phytotoxic effects of ozone using a stomatal flux-based parameterization, in which GPP impairment scales with both ambient ozone concentration and leaf stomatal conductance (Yue et al., 2024). Together, these combined aerosol and ozone effects explain the consistent suppression of GPP observed across southern China under varying sky conditions.

Are the simulation results consistent with observations? The observation-based data of GLASS gross primary productivity (GPP) and the Global Fire Emissions Database, version 4 s (GFED4s) were used to confirm the contribution of Indo-Chinese Peninsula (ICP) fire transport to GPP in southern China, through the differences between high and low fire emission years (Fig. 5). We selected eight years with the highest biomass burned and eight years with the lowest biomass burned, based on the average biomass burned in ICP during March-April from 1999 to 2014 (Fig. 5a). The years with high biomass burning (BB) emissions are 1999, 2004, 2005, 2007, 2010, 2012, 2013, and 2014, with an average emission of 2.74×10^7 kg of dry matter per month. The years with low BB emissions are 2000, 2001, 2002, 2003, 2006, 2008, 2009, and 2011, averaging 1.46×10^7 kg of dry matter per month. This represents a 47 % reduction compared to the years with higher BB emissions. Fig. 5a illustrates high GPP in years with low BB and low GPP in years with high BB, indicating the suppressive effect of BB on GPP in the three southern provinces of China during the ICP fire transport period, which is consistent with the simulated results described above. The difference in GPP in the three southern provinces of China between high and low biomass burning years in ICP is -0.24 gC m^{-2} d^{-1} (Fig. 5b), which is comparable to the model-simulated fire emission impact (Fig. 4). Furthermore, this value is slightly lower than the model-simulated fire emission impact, which is reasonable because fire emission transport still occurs during low fire years. All of these observation-based results support the model simulations.

While the observational results strongly support our model simulations, the environmental and ecological impacts of fire emission transport remain complex, influenced by multiple natural and anthropogenic factors. Lu et al. (Lu et al., 2025) used molecular markers to investigate temporal variations and source apportionment of biomass organic aerosols (BOAs) in the Pearl River Delta (PRD) region of China. Biomass burning emissions in Southeast Asia have been found to affect the PRD through long-range transport. The study indicates that geographic and anthropogenic factors—including the monsoon, plant phenology, and human activities—collectively influence the chemical composition of biomass burning and biomass burning organic aerosols (BOAs) in the PRD. Concurrently, aerosol-cloud interactions at higher altitudes significantly increase low cloud coverage over both land and ocean areas in tropical Southeast Asia (Ding et al., 2021). This phenomenon significantly reduces surface solar radiation, thereby limiting vegetation photosynthesis.

3.3. Changes of GPP by fire aerosols and ozone

3.3.1. Changes of GPP by fire aerosols

Aerosols can adjust surface photosynthetically active radiation (PAR) by altering both direct and diffuse solar radiation (Xia et al.,

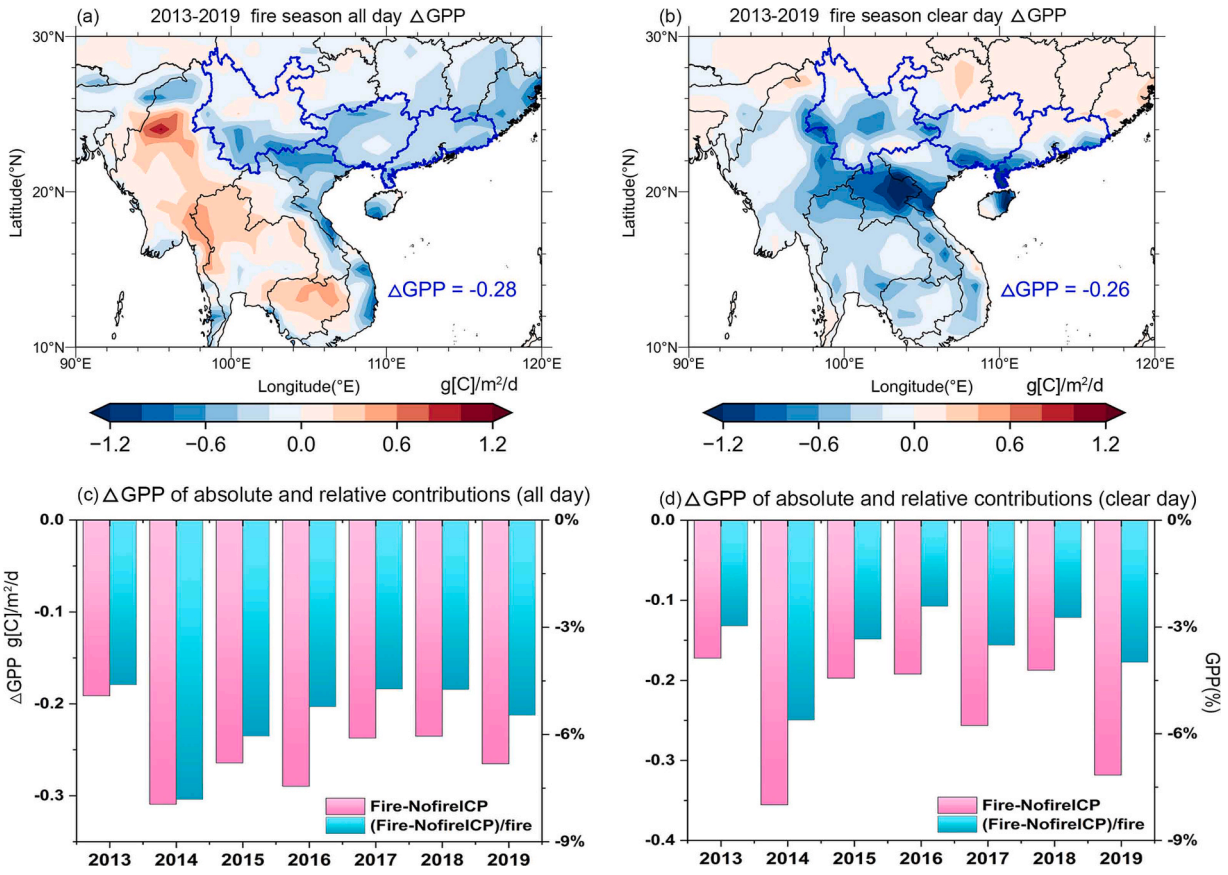

Fig. 4. The spatial distribution of the contributions of fire emissions in the Indo-Chinese Peninsula (ICP) region to gross primary productivity (GPP) during 2013–2019: (a) under all-sky condition and (b) under clear-sky condition; and the annual variation in the absolute and relative contributions of ICP fire transport to GPP in the three southern provinces of China for (c) all-sky condition and (d) clear-sky condition.

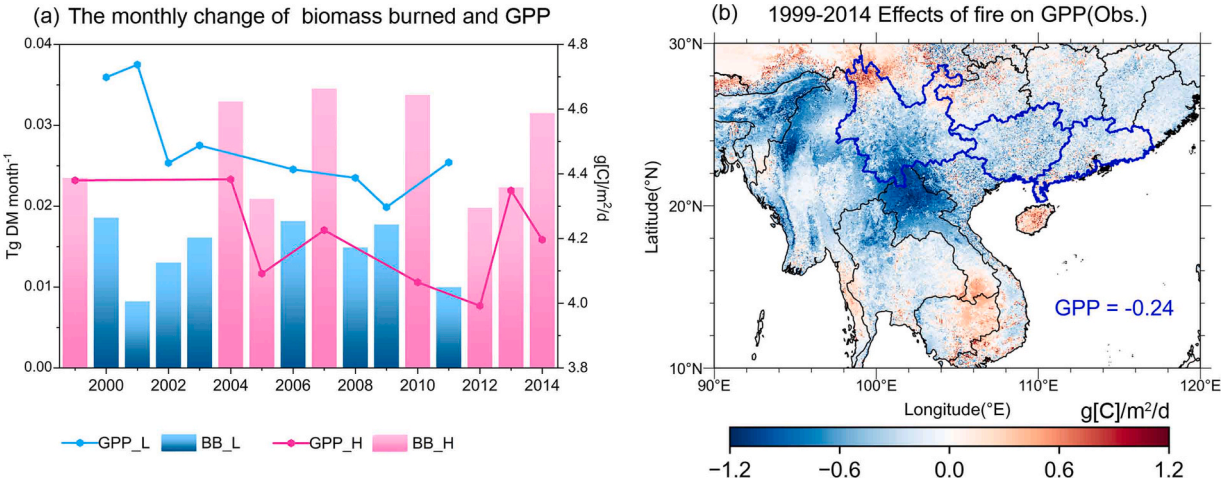

Fig. 5. (a) Response of gross primary productivity (GPP) in southern China to biomass burning emissions in Indo-Chinese Peninsula (ICP) region by the observation-based data of GLASS GPP and the Global Fire Emissions Database, version 4 s (GFED4s) fire emission. The GPP_H is the monthly average GPP in the three southern provinces of China with high monthly biomass burning years in ICP region (BB_H), while the GPP_L stands for the monthly average GPP in the three southern provinces of China with low monthly biomass burning years in ICP (BB_L); (b) Observation-based GPP difference between high and low biomass burning years in ICP.

2007). Fig. 6 illustrates the contributions of fire aerosols in the Indo-Chinese Peninsula (ICP) region to both diffuse and direct PAR in the three southern provinces of China (SC) and the ICP region during March–April from 2013 to 2019. For the ICP, fire aerosols increased diffuse PAR (Fig. 5a-b) while decreasing direct PAR (Fig. 5c-d). Across the ICP region, total PAR decreased by 0.30 W m^{-2} under all-sky conditions, with a more pronounced reduction of 2.26 W m^{-2} under clear-sky conditions. The transport of fire aerosols significantly affected PAR in downwind regions of southern China. For the three southern provinces of China, fire aerosols reduced total PAR through a combination of direct PAR attenuation and diffuse PAR enhancement. Fire aerosols caused a reduction in total surface PAR of 2.71 W m^{-2} under all-sky conditions and 1.71 W m^{-2} under clear-sky conditions. Under all-sky conditions, aerosols slightly reduced diffuse PAR by 0.03 W m^{-2}

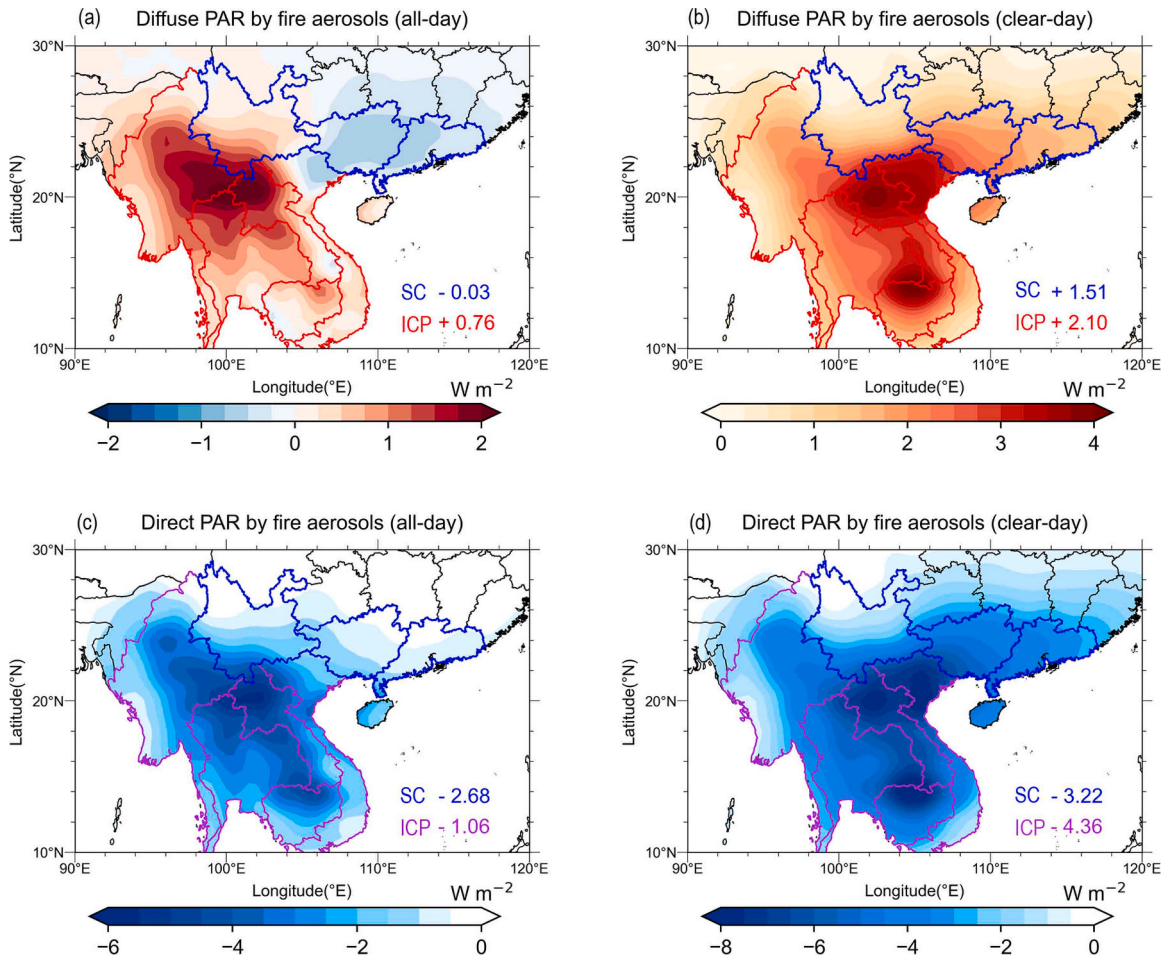

Fig. 6. The contributions of fire aerosols in the Indo-Chinese Peninsula (ICP) region to diffuse (first row) and direct (second row) photosynthetically active radiation (PAR) in the three southern provinces of China (SC) and ICP region during March-April 2013–2019, under all-sky condition (a, c) and clear-sky condition (b, d).

(Fig. 6a) while significantly decreasing direct PAR by 2.68 W m^{-2} (Fig. 6c). The effects were more pronounced under clear-sky conditions, with diffuse PAR increasing by 1.51 W·m^{-2} (Fig. 6b) and direct PAR dropping by 3.22 W·m^{-2} (Fig. 6d). Notably, under all-sky conditions, diffuse PAR was significantly reduced—a phenomenon consistently reported in previous studies (Chen and Zhuang, 2014a; Paulot et al., 2018; Rap et al., 2018). However, the relatively minor net changes in diffuse PAR changes under all-sky conditions observed in this study could be attributed to the effect of cloud modulation, where clouds alter radiative absorption and variably mitigate aerosol radiative effects (Paulot et al., 2018). Second, in terms of the net ecological effect, recent studies have confirmed that although aerosols alone can promote growth by increasing diffuse PAR, their combined effect with clouds leads to a sharp decrease in total PAR and causes more severe yield losses than clouds acting alone(Liu et al., 2025; Wang et al., 2025). Finally, the net aerosol radiative effect—whether it enhances or suppresses gross primary productivity (GPP)—is contingent upon an optimal aerosol load (Ezhova et al., 2018), where moderate levels boost photosynthesis but excess reduces it (Cox et al., 2008; Oliveira et al., 2007). This effect is strongest in dense-canopy forests, minimal in grasslands and croplands (Cheng et al., 2015; Kanniah et al., 2012; Niyogi et al., 2004), and is modulated by background cloudiness, as high cloud cover shifts the aerosol role from fertilization to dominant radiation attenuation, thereby suppressing GPP (Cheng et al., 2016).

Our study demonstrates that fire aerosols transported from the Indo-Chinese Peninsula (ICP) region significantly influence vegetation productivity in southern China by altering PAR, as shown in Fig. 7. Quantitative analysis reveals that transported fire aerosols reduced gross primary productivity (GPP) in the region by 0.27 gC m^{-2} d^{-1} under all-sky conditions (13.36 TgC per burning season), as shown in Fig. 7a, and by 0.25 gC m^{-2} d^{-1} under clear-sky conditions (12.18 TgC per burning season), as shown in Fig. 7b. Figs. 7c and 6d demonstrate significant interannual variability in aerosol-induced GPP suppression, with peak reductions occurring in 2014 under both all-sky and clear-sky conditions. This pattern closely aligns closely with the annual variability of biomass burning shown in Fig. 1b. The consistent covariation between biomass burning intensity and the magnitude of GPP reduction reinforces the causal relationship between fire aerosol transport and its impact on vegetation productivity in downwind regions.

The contrasting impacts of fire aerosols on local gross primary productivity (GPP) in ICP reveal an intriguing pattern: under all-sky conditions, they enhance GPP, whereas under clear-sky conditions, they suppress it. When diffuse radiation increases but total radiation continues to decrease, photosynthesis initially increases and then declines. Once direct radiation falls below a critical threshold, the gain from diffuse radiation can no longer compensate for the loss caused by reduced direct radiation, resulting in decreased GPP. This demonstrates the optimal concentration range for the aerosol diffuse radiation effect (Ezhova et al., 2018; Lu et al., 2017).

3.3.2. *Changes of GPP by fire O_3*

Ozone damage significantly threatens vegetation growth, and fire-induced ozone emissions negatively impact gross primary productivity (GPP). Fig. 8 shows the contributions of Indo-Chinese Peninsula (ICP) fire-induced ozone to GPP in the study region. During the fire season (March–April), biomass burning in the ICP region increases surface

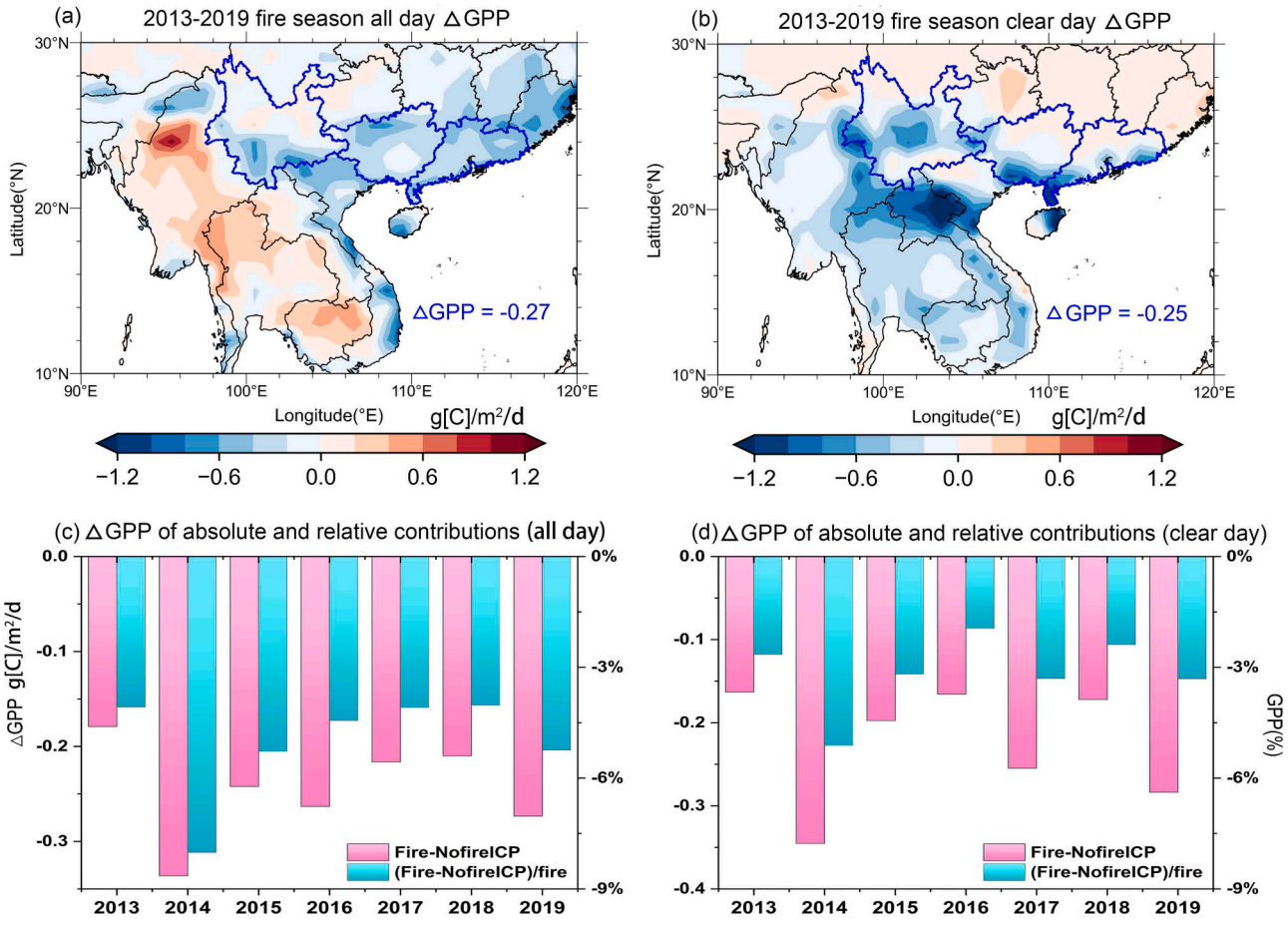

Fig. 7. The spatial distribution and annual variation of the absolute and relative contributions of Indo-Chinese Peninsula (ICP) fire aerosols to gross primary productivity (GPP) in the three southern provinces of China for (a, c) all-sky condition and (b, d) clear-sky condition.

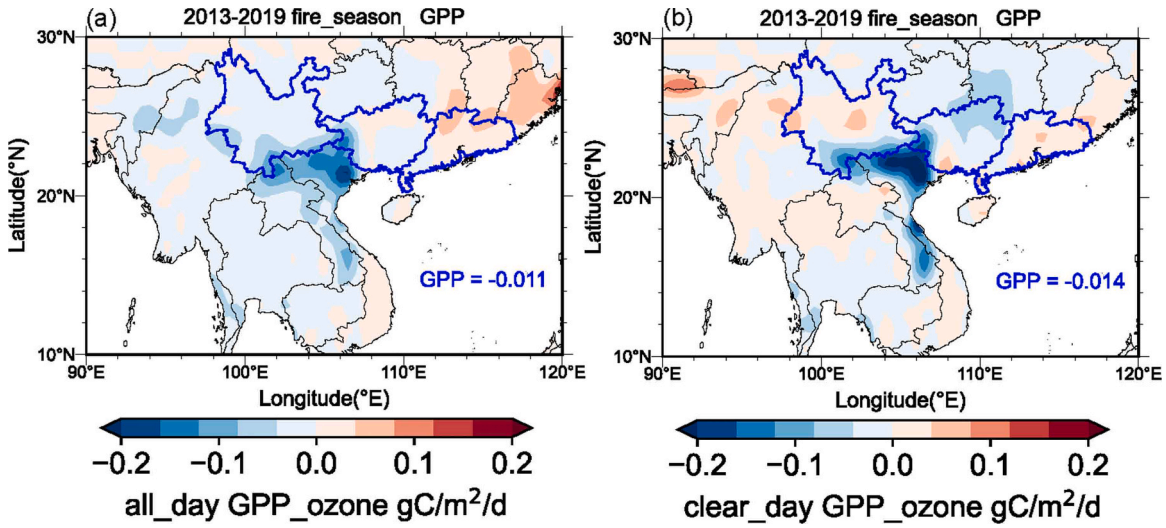

Fig. 8. Under all-sky condition (a) and clear-sky condition (b), the contributions of fire induced ozone in the Indo-Chinese Peninsula (ICP) region to gross primary productivity (GPP) during March-April 2013–2019. The blue values stand for regional means of GPP changes in three southern provinces of China.

ozone concentrations by 2.33 μg/m^3 in southern China. Our model simulations show that ozone causes relatively small but consistent reductions in GPP: 0.011 gC m^{-2} d^{-1} (-0.54 TgC per burning season) under all-sky conditions (Fig. 8a) and 0.014 gC m^{-2} d^{-1} (-0.69 TgC per burning season) under clear-sky conditions (Fig. 8b) in southern China. The ozone effects resulted in comparable reductions under both sky conditions. In the limited areas where GPP increased, the magnitude of this enhancement was indeed very small. This phenomenon results from the combined effects of ozone and aerosol concentrations, vegetation type, aerosol composition, meteorological conditions, and model uncertainties (Cheng et al., 2015; Kanniah et al., 2013; Shimizu et al., 2019).

The results of this study show that the gross primary productivity (GPP) loss caused by ozone under clear-sky conditions (-0.69 TgC) is higher than that under all-sky conditions (-0.54 TgC). This phenomenon is mainly attributed to the regulation of meteorological conditions on the effectiveness of ozone stress. The mechanism can be explained from two aspects: First, clear-sky conditions are usually accompanied by higher solar radiation intensity, air temperature, and lower air humidity. These environmental factors promote the opening of plant stomata (i.e., increase stomatal conductance) to maintain sufficient photosynthesis and transpiration (Dewar, 2006). However, the increase in stomatal conductance also provides a smoother channel for ozone to enter plants, leading to an increase in ozone uptake flux, which in turn causes more severe physiological damage and GPP reduction (Ainsworth et al., 2012; Fuhrer et al., 1997). Second, the stronger solar radiation and higher temperature under clear-sky conditions are also conducive to the occurrence of photochemical reactions (Atkinson, 2000; Sillman, 1999), thereby increasing ozone flux and concentration (Bai et al., 2025, 2017) and further exacerbating the exposure risk of vegetation. Therefore, the combined effect of higher stomatal conductance and potentially higher ozone concentration under clear-sky conditions results in more severe GPP loss.

4. Discussion

4.1. The impact of fire emissions on $PM_{2.5}$ and O_3

The southern provinces of China and the Indo-Chinese Peninsula (ICP) region are covered with various types of vegetation, where extensive biomass burning has been detected (Fig. 1a and Fig. 9a). Due to atmospheric circulation and monsoon patterns, the southern provinces of China were affected by air pollutants from fires. The impact of fire emissions transported in Southeast Asia has been investigated, as shown in Table 2. Biomass burning in Southeast Asia has significantly increased $PM_{2.5}$ and O_3 levels across southern China. Studies show $PM_{2.5}$ spikes of 39–73 μg/m^3 (17–78 %) in Yunnan and downwind provinces, with O_3 rising by 4–19 μg/m^3 (5–19 %). Regional fires contributed 10–80 % of $PM_{2.5}$ in southwestern China originating from Southeast Asia, with transboundary impacts from Mongolia, Russia, and Kazakhstan further increasing particulate pollution by 14 % and ozone levels by 8.6 % during biomass burning seasons.

In our study, the emissions from these fires significantly increased $PM_{2.5}$ and O_3 concentrations in the downwind southern provinces of China during March and April from 2013 to 2019 (Fig. 9b). Compared to $PM_{2.5}$ without fire aerosols, the mean $PM_{2.5}$ concentration increased from 43.69 μg/m^3 to 48.01 μg/m^3, representing an average increase of 9.0 %. This increase can be attributed to fire-induced pollutants. The mean O_3 also exhibited a similar increasing trend, rising by 2.5 % compared to O_3 without fire aerosols. The increases in $PM_{2.5}$ and O_3 concentrations caused by fire pollutants in this study were relatively

Table 2
Summary of previous studies about fire pollution transport.

Period	Source of the fires	Affected region	Results	References
March 21–25 2015	Southeast Asia	Yunnan Province	Biomass burning contributed + 39.3 μg m^{-3} (68.0 %) to $PM_{2.5}$ and + 18.1 μg m^{-3} (19.4 %) to O_3.	Xing et al. (2021)
March 21–25 2015	Southeast Asia	Downwind areas in southern China	Biomass burning contributed + 8.4 μg m^{-3} (24.1 %) to $PM_{2.5}$ and + 3.7 μg m^{-3} (5.3 %) to O_3.	Xing et al. (2021)
March-April 2013	Southeast Asia	Southwestern China	Fires contributed 10 %-40 % of the near-surface $PM_{2.5}$	Li et al. (2017a)
Open fire days in 2013–2021	Mongolia, Russia, Southeast Asia, and Kazakhstan.	China	Fire pollution contributed + 6.2 μg m^{-3} (14.1 %) to $PM_{2.5}$ and + 8.1 μg m^{-3} (8.6 %) to O_3.	Li et al. (2023)
March–April 2019	Southeast Asia	Kunming	Biomass burning contributed + 73.3 μg m^{-3} (78.0 %) to $PM_{2.5}$.	Fan et al. (2023)
Biomass burning days in 2009–2019	Southeast Asia	Guangdong-Hong Kong-Macao Great Bay Are	Biomass burning contributed + 29.27 μg m^{-3} (17.0 %) to $PM_{2.5}$.	Zeng et al. (2023)

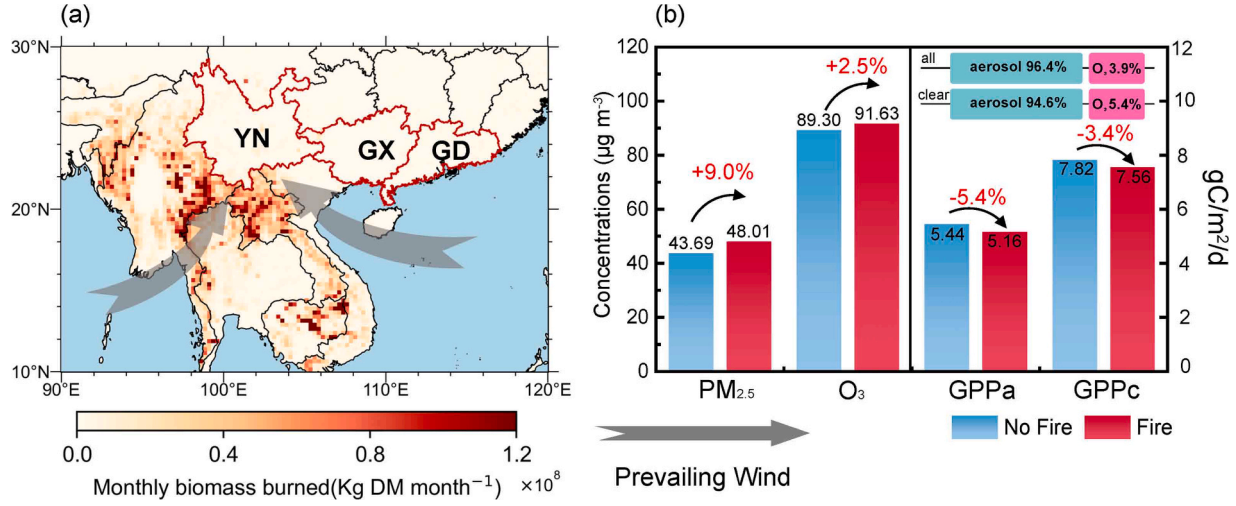

Fig. 9. (a) Spatial distributions of the biomass burned and main wind direction of the fire season. Identification of sources of fire emissions affecting provinces of southern China. The yellow grid cells represent the average monthly biomass burned for the corresponding grid cell from 2013 to 2019. The shades of grey represent main wind direction of the fire season from ERA5 data. (b)The emissions from these fires effectively increased $PM_{2.5}$ and O_3 concentrations and their contributions to gross primary productivity (GPP) in downwind the southern provinces of China.

lower than those reported in previous research. This discrepancy primarily arises from our methodological approach: instead of analyzing specific fire pollution events, we concentrated on the long-term effects of fires. This evaluation enables a more accurate assessment of the sustained impacts of fire pollutant transport on gross primary productivity (GPP). These fire pollutants emitted from biomass burning affect GPP in southern China through two key mechanisms: the aerosol radiation effect and the ozone damage effect. We quantify the percentage changes in GPP in the southern provinces of China caused by biomass burning. Compared to GPP changes without biomass burning, fire pollution decreased GPP by 5.4 % under all-sky conditions and by 3.4 % under clear-sky conditions (Fig. 9b). The fire aerosols contributed to 96.4 % of the GPP reduction under all-sky conditions and 94.6 % under clear-sky conditions, whereas ozone damage played a minor role, accounting for only 3.9 % under all-sky conditions and 5.4 % under clear-sky conditions of the GPP decline. Studies have reported divergent impacts of fire emissions on GPP. Yue and Unger (2018) observed a slight global increase in GPP (0.05–0.07 Pg C yr^{-1}), whereas Xu et al. (2021) estimated a net global reduction of 2.8 Pg C yr^{-1} . Regionally, Xie et al. (2020) found that aerosols enhanced GPP by 0.36 Pg C yr^{-1} in southern China. These discrepancies primarily result from variations in vegetation type, canopy structure, aerosol loading, and cloud cover across regions, all of which influence the GPP response to fire aerosols (Ezhova et al., 2018; Lu et al., 2017). There may also be a more important reason: previous studies primarily examined the annual-scale impacts of global fire emissions on GPP, which mainly affect the source area. In contrast, our study specifically investigates fire emissions during the peak burning season (March–April) and emphasizes the influence of regional aerosol transport on GPP in downwind areas.

4.2. Uncertainties

The conclusions of this study are based on the model chain, and it is crucial to identify its uncertainties. The evaluation results reveal that the model systematically overestimates surface $PM_{2.5}$ and O_3 concentrations (Fig. 3a–b), yet underestimates column AOD (Fig. 3c). This AOD underestimation can lead to a corresponding overestimation of shortwave radiation at the surface (Fig. 3d–e). Taken together, these findings point to inaccuracies in the simulated vertical distribution of pollutants. The overestimated shortwave radiation may either enhance or reduce the simulated gross primary productivity (GPP), while elevated O_3 concentrations are likely to suppress it (Li et al., 2015; Wang et al., 2023). As a result, these opposing effects may partially offset each other in the GPP simulations. Nevertheless, the overall GPP evaluation shows reasonably good agreement with observations (R = 0.88, MB = 0.3 in Fig. 3f).

It should also be noted that this study focuses on the contribution of fire emissions—specifically, the relative differences between simulations with and without fires—rather than on absolute model outputs. Therefore, the accuracy of the fire emission inventory is critical. Here, we employ the Global Fire Emissions Database, version 4 s (GFED4s) inventory, which is widely used and has been extensively evaluated (Akagi et al., 2011; Giglio et al., 2013). In addition, the model reproduces the interannual variability of pollutant concentrations fairly well (Fig. 3b), supporting its applicability for analyzing regional-scale interannual variations.

In summary, although there is room for improvement in the absolute accuracy of the model, these uncertainties are more likely to affect the absolute values of GPP loss estimates rather than reverse the qualitative conclusion regarding the relative relationship—"fire emissions cause damage to GPP". Future work will further constrain model uncertainties.

This study evaluates the combined effects of aerosols and ozone on gross primary productivity (GPP) in Southern China, a region encompassing diverse ecosystems ranging from evergreen broad-leaved forests to croplands (Fig. 1a). Tall, closed forests benefit more from aerosol-induced diffuse radiation, while shallow-canopy crops or grasslands see limited gains (Cheng et al., 2015; Kanniah et al., 2012; Niyogi et al., 2004). Conversely, broadleaved trees and C3 crops with higher stomatal conductance suffer greater ozone damage due to higher uptake (Wang et al., 2025). Therefore, the varying responses of different vegetation types to fire emissions cause spatially heterogeneous impacts, necessitating future attribution analysis by plant functional type.

5. Conclusions

We analyzed the impacts of transboundary pollutants from biomass burning in Indo-Chinese Peninsula (ICP) on southern China's gross primary productivity (GPP) during March and April from 2013 to 2019. During the peak fire emission season (March-April, 2013–2019), biomass burning in the ICP reduced GPP in three southern Chinese provinces by 0.28 gC m^{-2} d^{-1} (an annual mean reduction of 5.4 %) under all-sky conditions and by 0.26 gC m^{-2} d^{-1} (an annual mean reduction of 3.4 %) under clear-sky conditions. Among these reductions, under all-sky conditions, aerosol radiative effects accounted for 96.4 % of the GPP reduction, while O_3 damage contributed 3.9 %. Under clear-sky conditions, aerosol radiative effects accounted for 94.6 % of the reduction in GPP, whine O_3 damage was responsible for the remaining 5.4 %. Fire aerosols transported from the ICP significantly altered photosynthetically active radiation (PAR) in southern China, with direct PAR decreasing by 2.68 W/m^2 under all-sky conditions and by 3.22 W/m^2 under clear-sky conditions. In contrast, diffuse PAR was −0.03 W/m^2 under all-sky conditions but + 1.51 W/m^2 under clear-sky conditions. Biomass burning emissions from ICP significantly increased aerosol and O_3 levels in three southern Chinese provinces. $PM_{2.5}$ concentrations increased by 9.0 % (from 43.69 to 48.01 μg/m^3), with this rise attributed to fire emissions. Ozone showed a similar increase, rising by 2.5 % (from 89.30 to 91.63 μg/m^3) compared to fire-free conditions.

This study quantitatively assessed the multi-year impacts of Indo-Chinese Peninsula (ICP) biomass burning on vegetation productivity in southern China using model simulations. Potential uncertainties in the simulations may arise from limitations in model resolution, variations in aerosol composition, and changes in land cover. This study did not fully account for recent land-use changes in both the Indochina Peninsula and southern China, which could affect influence the simulation results. due to the accessibility of ground-based observation data, the model validation in this study is mainly concentrated in Southern China. Future research should incorporate ground-based observations from a broader geographic area and quantify the interconnected physicochemical processes of fire emissions and land-use changes to improve model-based assessments of ecological impacts and vegetation dynamics.

Author contributions

JZ conceived the study. JZ and WY designed the research, conducted the data analysis, and wrote the paper. YoH, JiZ, XC, SY and HW provided advice on writing the paper and helped with data analysis procedures. XY, CT, YiH, YZ and HL provided scientific advice. All co-authors contributed to improving the paper.

CRediT authorship contribution statement

Sheng Yang: Visualization, Data curation. **Yonghang Hu:** Visualization, Methodology, Data curation. **Chenguang Tian:** Supervision, Project administration, Investigation, Data curation. **Xu Yue:** Validation, Supervision, Project administration, Methodology, Funding acquisition, Conceptualization. **Jun Zhu:** Writing – review & editing, Visualization, Validation, Supervision, Project administration, Methodology, Funding acquisition, Formal analysis, Data curation, Conceptualization. **Hong Liao:** Supervision, Project administration, Funding acquisition. **Wenjie Yan:** Writing – review & editing, Writing – original draft, Visualization, Validation, Resources, Methodology, Formal analysis, Data curation. **Yuan Zhao:** Visualization. **Yihan Hu:** Visualization.

Xin Chen: Visualization. **Jiao Zheng:** Visualization, Data curation. **Haoyu Wei:** Visualization, Methodology.

Declaration of Competing Interest

In accordance with your policy, we hereby declare that the authors have no known competing financial interests or personal relationships that could have appeared to influence the work reported in this paper. We have no relevant interests to declare, including but not limited to: employment, consultancies, stock ownership, honoraria, paid expert testimony, patent applications/registrations, grants, or other funding. Furthermore, no author is affiliated with the journal in an editorial or advisory capacity.

Acknowledgements

The authors acknowledge financial support from the National Key Research and Development Program of China (grant no. 2023YFF0805402), the National Natural Science Foundation of China (grant no. 42030608), the National Natural Science Foundation of China (grant no. 42575197), and the Jiangsu Science Fund for Carbon Neutrality (grant BK20220031).

Data availability

Data will be made available on request.

References

Ainsworth, E.A., et al., 2012. The effects of tropospheric ozone on net primary productivity and implications for climate change. Annu Rev. Plant Biol. 63, 637–661.
Akagi, S.K., et al., 2011. Emission factors for open and domestic biomass burning for use in atmospheric models. Atmos. Chem. Phys. 11, 4039–4072.
Atkinson, R., 2000. Atmospheric chemistry of VOCs and NO_x. Atmos. Environ. 34, 2063–2101.
Azevedo, J.M., et al., 2011. Long-range ozone transport and its impact on respiratory and cardiovascular health in the north of Portugal. Int. J. Biometeorol. 55, 187–202.
Bai, J.H., et al., 2017. Seasonal and interannual variations in whole-ecosystem BVOC emissions from a subtropical plantation in China. Atmos. Environ. 161, 176–190.
Bai, J., et al., 2025. Seasonal variations in whole–ecosystem BVOC emissions and ozone fluxes from a tropical rubber tree plantation in China. Atmos. Environ. 351.
Bencherif, H., et al., 2020. Investigating the long-range transport of Aerosol Plumes following the amazon fires (August 2019): a multi-instrumental approach from ground-based and satellite observations. Remote Sens. 12.
Bhawar, R.L., et al., 2024. Aerosol emission patterns from the february 2019 Karnataka fire. Fire 7.
Brown, H., et al., 2021. Biomass burning aerosols in most climate models are too absorbing. Nat. Commun. 12.
Chan, C.Y., et al., 2003. Characteristics of biomass burning emission sources, transport, and chemical speciation in enhanced springtime tropospheric ozone profile over Hong Kong. J. Geophys. Res. Atmospheres 108.
Chang, C.H., et al., 2015. Evaluating spatial and temporal variations of Aerosol optical depth and biomass burning over southeast asia based on satellite data products. Aerosol Air Qual. Res. 15, 2625–2640.
Chen, J.M., et al., 2017. A review of biomass burning: Emissions and impacts on air quality, health and climate in China. Sci. Total Environ. 579, 1000–1034.
Chen, M., Zhuang, Q., 2014a. Evaluating aerosol direct radiative effects on global terrestrial ecosystem carbon dynamics from 2003 to 2010. Tellus B Chem. Phys. Meteorol. 66.
Chen, M., Zhuang, Q.L., 2014b. Evaluating aerosol direct radiative effects on global terrestrial ecosystem carbon dynamics from 2003 to 2010. Tellus Ser. B Chem. Phys. Meteorol. 66.
Cheng, S.J., et al., 2015. Variations in the influence of diffuse light on gross primary productivity in temperate ecosystems. Agric. For. Meteorol. 201, 98–110.
Cheng, S.J., et al., 2016. Using satellite-derived optical thickness to assess the influence of clouds on terrestrial carbon uptake. J. Geophys. Res. Biogeosci. 121, 1747–1761.
Choi, M., Ying, Q., 2025. Modeling the impacts of open biomass burning on regional O_3 and PM $_{2.5}$ in Southeast Asia considering light absorption and photochemical bleaching of Brown carbon. Atmos. Environ. 342.
Coen, J., 2018. Some requirements for simulating wildland fire behavior using insight from coupled weather-wildland fire models. Fire 1.
Cohen, J.B., et al., 2017. Decadal-scale relationship between measurements of aerosols, land-use change, and fire over Southeast Asia. Atmos. Chem. Phys. 17, 721–743.
Cox, P.M., et al., 2008. Increasing risk of Amazonian drought due to decreasing aerosol pollution. Nature 453.
Dewar, R.C., 2006. Interpretation of an empirical model for stomatal conductance in terms of guard cell function. Plant Cell Environ. 18, 365–372.
Ding, A.J., et al., 2013. Intense atmospheric pollution modifies weather: a case of mixed biomass burning with fossil fuel combustion pollution in eastern China. Atmos. Chem. Phys. 13, 10545–10554.
Ding, K., et al., 2021. Aerosol-boundary-layer-monsoon interactions amplify semi-direct effect of biomass smoke on low cloud formation in Southeast Asia. Nat. Commun. 12.
Ezhova, E., et al., 2018. Direct effect of aerosols on solar radiation and gross primary production in boreal and hemiboreal forests. Atmos. Chem. Phys. 18, 17863–17881.
Fan, W.X., et al., 2023. Impacts of biomass burning in Southeast Asia on aerosols over the low-latitude plateau in China: an analysis of a typical pollution event. Front. Environ. Sci. 11.
Feng, Z.Z., et al., 2018. A unifying explanation for variation in ozone sensitivity among woody plants. Glob. Change Biol. 24, 78–84.
Feng, Z.Z., et al., 2022. Ozone pollution threatens the production of major staple crops in East Asia. Nat. Food 3, 47.
Friedlingstein, P., et al., 2025. Global carbon budget 2024. Earth Syst. Sci. Data 17, 965–1039.
Fu, J.S., et al., 2012. Evaluating the influences of biomass burning during 2006 BASE-ASIA: a regional chemical transport modeling. Atmos. Chem. Phys. 12, 3837–3855.
Fuhrer, J., et al., 1997. Critical levels for ozone effects on vegetation in Europe. Environ. Pollut. 97, 91–106.
Giglio, L., et al., 2013. Analysis of daily, monthly, and annual burned area using the fourth-generation global fire emissions database (GFED4). J. Geophys. Res. Biogeosci. 118, 317–328.
Giorgi, F., et al., 2012. RegCM4: model description and preliminary tests over multiple CORDEX domains. Clim. Res. 52, 7–29.
Haofan, T.A.N.G., X, Y., Jianlin, A.I., 2019. Carbon storage and carbon density of forest vegetation and their spatial distribution pattern in Yunnan Province. For. Resour. Wanagement 5, 37–43.
Hein, L., et al., 2022. The health impacts of Indonesian peatland fires. Environ. Health 21.
Hu, W.Y., et al., 2023. Changing Responses of $PM_{2.5}$ and Ozone to Source Emissions in the Yangtze River Delta Using the Adjoint Model. Environ. Sci. Technol. 58, 628–638.
Huang, K., et al., 2013. Impact assessment of biomass burning on air quality in Southeast and East Asia during BASE-ASIA. Atmos. Environ. 78, 291–302.
Huang, X., et al., 2016. Effects of aerosol-radiation interaction on precipitation during biomass-burning season in East China. Atmos. Chem. Phys. 16, 10063–10082.
Hung, W.T., et al., 2021. The impacts of transported wildfire smoke aerosols on surface air quality in New York State: A multi-year study using machine learning. Atmos. Environ. 259.
Jiang, Z.J., et al., 2020. Spatiotemporal and probability variations of surface $PM_{2.5}$ over China between 2013 and 2019 and the associated changes in health risks: An integrative observation and model analysis. Sci. Total Environ. 723.
Kanniah, et al., 2012. Control of atmospheric particles on diffuse radiation and terrestrial plant productivity: A review. Prog. Phys. Geogr. Earth Environ. 24, 209–237.
Kanniah, K.D., et al., 2013. Exploring the link between clouds, radiation, and canopy productivity of tropical savannas. Agric. For. Meteorol. 182, 304–313.
Keller, C.A., et al., 2014. HEMCO v1.0: a versatile, ESMF-compliant component for calculating emissions in atmospheric models. Geosci. Model Dev. 7, 1409–1417.
Kommula, S.M., et al., 2024. Effect of Long-Range Transported Fire Aerosols on Cloud Condensation Nuclei Concentrations and Cloud Properties at High Latitudes. Geophys. Res. Lett. 51.
Kong, S.S.K., et al., 2022. Distinct transport mechanisms of East Asian dust and the impact on downwind marine and atmospheric environments. Sci. Total Environ. 827.
Lan, X., D, H., Song, T.Q., Zeng, F.P., Peng, W.X., Liu, Y.X., Fan, Z.L., Zhang, J.Y., 2019. Vegetation carbon storage in the main forest types in Guangxi and the related influencing factors. Acta Ecol. Sin. 39 (6).
Li, D., et al., 2015. Impact of estimated solar radiation on gross primary productivity simulation in subtropical plantation in southeast China. Sol. Energy 120, 175–186.
Li, J., et al., 2017a. Regional Impact of Biomass Burning in Southeast Asia on Atmospheric Aerosols during the 2013 Seven South-East Asian Studies Project. Aerosol Air Qual. Res. 17, 2924–2941.
Li, M., et al., 2017b. MIX: a mosaic Asian anthropogenic emission inventory under the international collaboration framework of the MICS-Asia and HTAP. Atmos. Chem. Phys. 17, 935–963.
Li, X., et al., 2023. Aggravated multi-source air pollution exposure caused by open fires in China. J. Clean. Prod. 394.
Li, J.W., et al., 2024. Impacts of vertical distribution of Southeast Asian biomass burning emissions on aerosol distributions and direct radiative effects over East Asia. Atmos. Environ. 318.
Lin, C.Y., et al., 2014a. Modelling of long-range transport of Southeast Asia biomass-burning aerosols to Taiwan and their radiative forcings over East Asia. Tellus Ser. BChem. Phys. Meteorol. 66.
Lin, N.H., et al., 2014b. Interactions between biomass-burning aerosols and clouds over Southeast Asia: Current status, challenges, and perspectives. Environ. Pollut. 195, 292–307.
Lin, H.P., et al., 2021. Harmonized Emissions Component (HEMCO) 3.0 as a versatile emissions component for atmospheric models: application in the GEOS-Chem, NASA GEOS, WRF-GC, CESM2, NOAA GEFS-Aerosol, and NOAA UFS models. Geosci. Model Dev. 14, 5487–5506.
Lin, J.-T., McElroy, M.B., 2010. Impacts of boundary layer mixing on pollutant vertical profiles in the lower troposphere: Implications to satellite remote sensing. Atmos. Environ. 44, 1726–1739.

Lin, S., Rood, R.B., 1996. Multidimensional Flux-Form Semi-Lagrangian Transport Schemes. Mon. Weather Rev. 124, 2046–2070.
Liu, H., et al., 2001. Constraints from 210Pb and 7Be on wet deposition and transport in a global three-dimensional chemical tracer model driven by assimilated meteorological fields. J. Geophys. Res. Atmospheres 106, 12109–12128.
Liu, Y., et al., 2025. Quantifying the effects of aerosols and cloud radiative effect on rice growth and yield. Agric. For. Meteorol. 364.
Lu, X.L., et al., 2017. Enhanced water use efficiency in global terrestrial ecosystems under increasing aerosol loadings. Agric. For. Meteorol. 237, 39–49.
Lu, X.M., et al., 2019. Investigating Smoke Aerosol Emission Coefficients Using MODIS Active Fire and Aerosol Products: A Case Study in the CONUS and Indonesia. J. Geophys. Res. Biogeosci. 124, 1413–1429.
Lu, L.X., et al., 2025. Temporal Variations and Source Apportionment of Biomass Burning and Biogenic Organic Aerosols in the Pearl River Delta: Effects of the Monsoon, Plant Phenology, and Anthropogenic Activities. J. Geophys. Res. Atmospheres 130.
Mahowald, N., 2011. Aerosol Indirect Effect on Biogeochemical Cycles and Climate. Science 334, 794–796.
Martins, V.S., et al., 2018. Seasonal and interannual assessment of cloud cover and atmospheric constituents across the Amazon (2000-2015): Insights for remote sensing and climate analysis. Isprs J. Photogramm. Remote Sens. 145, 309–327.
Niyogi, D., et al., 2004. Direct observations of the effects of aerosol loading on net ecosystem CO2 exchanges over different landscapes. Geophys. Res. Lett. 31.
Oliveira, P.H.F., et al., 2007. The effects of biomass burning aerosols and clouds on the CO_2 flux in Amazonia. Tellus B Chem. Phys. Meteorol. 59.
Park, C.Y., et al., 2024. Attributing human mortality from fire $PM_{2.5}$ to climate change. Nat. Clim. Change 14.
Paulot, F., et al., 2018. Changes in the aerosol direct radiative forcing from 2001 to 2015: observational constraints and regional mechanisms. Atmos. Chem. Phys. 18, 13265–13281.
Pereira, G., et al., 2009. Estimating trace gas and aerosol emissions over South America: Relationship between fire radiative energy released and aerosol optical depth observations. Atmos. Environ. 43, 6388–6397.
Rap, A., et al., 2018. Enhanced global primary production by biogenic aerosol via diffuse radiation fertilization. Nat. Geosci. 11, 640–644.
Reddington, C.L., et al., 2014. Contribution of vegetation and peat fires to particulate air pollution in Southeast Asia. Environ. Res. Lett. 9.
Reddington, C.L., et al., 2021. Air Pollution From Forest and Vegetation Fires in Southeast Asia Disproportionately Impacts the Poor. Geohealth 5.
Shimizu, Y., et al., 2019. A novel remote sensing-based method of ozone damage assessment effect on Net Primary Productivity of various vegetation types. Atmos. Environ. 217.
Sillman, S., 1999. The relation between ozone, NO_x and hydrocarbons in urban and polluted rural environments. Atmos. Environ. 33, 1821–1845.
Tian, C., et al., 2023. Projections of fire emissions and the consequent impacts on air quality under 1.5 °C and 2 °C global warming. Environ. Pollut. 323.
Tsay, S.C., et al., 2013. From BASE-ASIA toward 7-SEAS: A satellite-surface perspective of boreal spring biomass-burning aerosols and clouds in Southeast Asia. Atmos. Environ. 78, 20–34.
van der Werf, G.R., et al., 2017. Global fire emissions estimates during 1997-2016. Earth Syst. Sci. Data 9, 697–720.
Videla, F.C., et al., 2013. The relative role of Amazonian and non-Amazonian fires in building up the aerosol optical depth in South America: A five year study (2005-2009). Atmos. Res. 122, 298–309.
Wang, Y., et al., 1998. Global simulation of tropospheric O_3-NOx-hydrocarbon chemistry: 1. Model formulation. J. Geophys. Res. Atmospheres 103, 10713–10725.
Wang, X.L., et al., 2022. Rapidly changing emissions drove substantial surface and tropospheric ozone increases over Southeast Asia. Geophys. Res. Lett. 49.
Wang, Y., et al., 2023. The impacts of ambient ozone pollution on China's wheat yield and forest production from 2010 to 2021. Environ. Pollut. 330.
Wang, Y., et al., 2025. A Meta-Analysis of the Response of Leaf Photosynthesis Rate to Tropospheric Ozone. Clim. Environ. Res. 30, 212–224.
Wei, J., et al., 2023. Spring biomass burning in Indochina enhances summer Yangtze River Valley rainfall through land–atmosphere interactions. npj Clim. Atmos. Sci. 6.
Wesely, M.L., 1989. Parameterization of surface resistances to gaseous dry deposition in regional-scale numerical models. Atmos. Environ. 23, 1293–1304.
WotawaTrainer, 2000. The influence of canadian forest fires on pollutant concentrations in the united states. Science 288, 324–328.
Wu, S., et al., 2007. Why are there large differences between models in global budgets of tropospheric ozone? J. Geophys. Res. Atmospheres 112.
Xia, X., et al., 2007. Estimation of aerosol effects on surface irradiance based on measurements and radiative transfer model simulations in northern China. J. Geophys. Res. Atmospheres 112.
Xie, X., et al., 2020. Effects of atmospheric aerosols on terrestrial carbon fluxes and CO_2 concentrations in China. Atmos. Res. 237.
Xing, L., et al., 2021. Impacts of biomass burning in peninsular Southeast Asia on $PM_{2.5}$ concentration and ozone formation in Southern China during springtime—a case study. J. Geophys. Res., Atmos. 126.
Xu, L., et al., 2021. The influence of fire aerosols on surface climate and gross primary production in the Energy Exascale Earth System Model (E3SM). J. Clim. 1–60.
Yang, Q.J., et al., 2022. The cross-border transport of $PM_{2.5}$ from the southeast asian biomass burning emissions and its impact on air pollution in Yunnan Plateau, Southwest China. Remote Sens. 14.
Yin, Y., et al., 2020. Fire decline in dry tropical ecosystems enhances decadal land carbon sink. Nat. Commun. 11.
Yin, X., et al., 2021. Influence of transboundary air pollution on air quality in southwestern China. Geosci. Front. 12.
Youn, D., et al., 2011. Impacts of aerosols on regional meteorology due to Siberian forest fires in May 2003. Atmos. Environ. 45, 1407–1412.
Yue, X., et al., 2010. Simulation of dust aerosol radiative feedback using the GMOD: 2. Dust-climate interactions. J. Geophys. Res. Atmospheres 115.
Yue, X., et al., 2015. Distinguishing the drivers of trends in land carbon fluxes and plant volatile emissions over the past 3 decades. Atmos. Chem. Phys. 15, 11931–11948.
Yue, X., et al., 2017. Ozone and haze pollution weakens net primary productivity in China. Atmos. Chem. Phys. 17, 6073–6089.
Yue, X., et al., 2024. Development and evaluation of the interactive Model for Air Pollution and Land Ecosystems (iMAPLE) version 1.0. Geosci. Model Dev. 17, 4621–4642.
Yue, X., Liao, H., 2012. Climatic responses to the shortwave and longwave direct radiative effects of sea salt aerosol in present day and the last glacial maximum. Clim. Dyn. 39, 3019–3040.
Yue, X., Unger, N., 2017. Aerosol optical depth thresholds as a tool to assess diffuse radiation fertilization of the land carbon uptake in China. Atmos. Chem. Phys. 17, 1329–1342.
Yue, X., Unger, N., 2018. Fire air pollution reduces global terrestrial productivity. Nat. Commun. 9.
Zeng, X., et al., 2023. CALIPSO-observed Southeast Asia biomass-burning influences on aerosol vertical structure in Guangdong-Hong Kong-Macao Greater Bay Area. Atmospheric Research 289.
Zhang, et al., 2001. A size-segregated particle dry deposition scheme for an atmospheric aerosol module. Atmos. Environ. 35, 549–560.
Zhang, X.T., et al., 2021. Three-dimensional spatiotemporal evolution of wildfire-induced smoke aerosols: A case study from Liangshan, Southwest China. Sci. Total Environ. 762.
Zhang, L.J., et al., 2022. The impact of long-range transport of biomass burning emissions in southeast asia on Southern China. Atmosphere 13.
Zhang, L., L, W.H., Wang, Z., Yu, N., Chen, H.Y., 2010. Spatial distribution pattern of carbon storage in forest vegetation of Guangdong province. Ecol. Environ. Sci. 19 (6), 1295–1299.
Zhang Yuxing, W.X., Pu, Ying, 2021. Changes in forest resource carbon storage in China between 1949 and 2018. J. Beijing For. Univ. 43 (5), 1–14.
Zheng, H.Y., et al., 2023. ENSO-related fire weather changes in southeast and equatorial asia: a quantitative evaluation using fire weather index. J. Geophys. Res. Atmos. 128.
Zhu, J., et al., 2022. Contribution of Fire Emissions to $PM_{2.5}$ and Its Transport Mechanism Over the Yungui Plateau, China During 2015-2019. J. Geophys. Res. Atmos. 127.
Zhu, J., et al., 2024. The multi-year contribution of Indo-China peninsula fire emissions to aerosol radiation forcing in southern China during 2013-2019. Sci. Total Environ. 927.